

# The Influence of Spar Location on the Elastic Deformation and the Weight Estimation of a Swept-back, High Altitude, Solar Powered Flying Wing UAV

Ahmad Alsahlani \* and Thurai Rahulan \*\*

University of Salford, School of Computing, Science & Engineering  
Salford, Greater Manchester, M5 4WT, United Kingdom

\* [ahmad.alsahlani@gmail.com](mailto:ahmad.alsahlani@gmail.com)

\*\* [t.rahulan@salford.ac.uk](mailto:t.rahulan@salford.ac.uk)

## Abstract

In this paper, a design procedure is introduced for an aft swept flying wing aircraft to study the influence of the spar location on the performance of the resulting wing geometry. The study was conducted using an in-house low fidelity design/optimisation tool which was built within the MATLAB environment. The tool consists of a quasi-3D aerodynamics model and a composite structure model in addition to an optimiser code. The case study involves a swept-back solar-powered flying wing UAV. Four design cases with different spar location were introduced and the results of these cases were then compared. The main finding was that the spar location has an enormous impact on the structural behaviour and thus the aerodynamic performance and stability. Moreover, if the spar location was behind the aerodynamic centre line, the wing torsion due to aerodynamic loads can mitigate the elastic deflection in a beneficial manner to enhance the stability. However, this will result in greater structural weight.

## 1. Introduction

High-altitude aircraft flying in the stratosphere and characterised by ultra-light and high aspect ratio wings result in very flexible airframes. Most of the existing solar powered high altitude aircraft have straight wings such as the Helios, Pathfinder and Centriano built by NASA. The aeroelastic properties of these aircraft have of course been investigated in the past. However, a swept back flying wing configuration has not been studied for high aspect ratio wing configuration. Sustained flight at high altitudes involves a range of difficulties such as low temperature and low air density. These physical properties of the air impact upon the ability of the vehicle to generate sufficient aerodynamic lift to support the weight. Moreover, the low air density at high altitudes will result in significantly reduced generation of thrust from air-breathing propulsion systems [1]. There can also be significant challenges in achieving satisfactory stability and control characteristics for the vehicle when operating at high altitudes.

In general, high altitude aircraft have large wingspans and the low mass will make it flexible [2]. Therefore, the aerodynamic loads will considerably influence the wing shape and this, in turn, will affect the aerodynamic performance and the stability of the aircraft. If the deflections become large, the aeroelastic behaviour will significantly modify and possibly lead to nonlinear aeroelastic behaviour [3, 4].

Structurally, it is convenient to consider the bending moment about an axis perpendicular to the elastic axis (spar locus) whilst the local angles of attack (incidences) are measured with respect to the free flow direction [5]. In the case of applying pure up-bending load on an aft-swept wing, a decrease of the local wing incidence is produced due to the differences in the elastic vertical displacements at the leading and trailing edges as shown in Figure 1. This influence is reversed in the case of down bending of the wing, leading to an increase in the effective incidence. Therefore, the elastic twist of the wing under flight condition will be a part of the elastic twist and the bending deflection [6, 7].

There are two main sets of challenges facing the design process to achieve the stability of such high-altitude aircraft associated with the layout configuration and structural deformations. The first challenge concerning tailless aircraft configuration, necessitates the offering of an alternative design feature to enhance the stability such as sweeping and/or twisting of the wing in addition to using variations in aerofoils. The second set of challenges is associated with the elastic behaviour exhibited by the structure of high altitude aircraft which impacts the aerodynamic forces and moments, and thus stability. For swept flying wing, the elastic deformation can shift the aerodynamic centre forwards, which in return reduces the longitudinal static stability [8]. Also, this can influence the slope of the lift curve leading to an increase in the trimmed angle of attack. These effects become worse with increasing the sweep angle and the aspect ratio of the wing. Studies conducted on conventional aircraft with swept wings concluded that the torsional deflections had a stabilising influence whilst the bending deformations tended to destabilise [8]. The

overall effect of these two influences is dependent on the sweep angle, the location of the spar and the ratio of bending to torsional stiffness values. Moreover, the static and dynamic aeroelastic effects will significantly affect the aircraft flight dynamics [3]. However, these factors are not the focus in this paper.

In previous research conducted by the authors, an optimisation design and a conceptual design tool were built to study the challenges encountered when designing a high altitude aft swept flying wing UAV. These tools have been used to conduct the work presented in this paper as will be discussed later. Moreover, the main characteristics of the aircraft case study were taken from results obtained by the conceptual design tool detailed in [9-11].

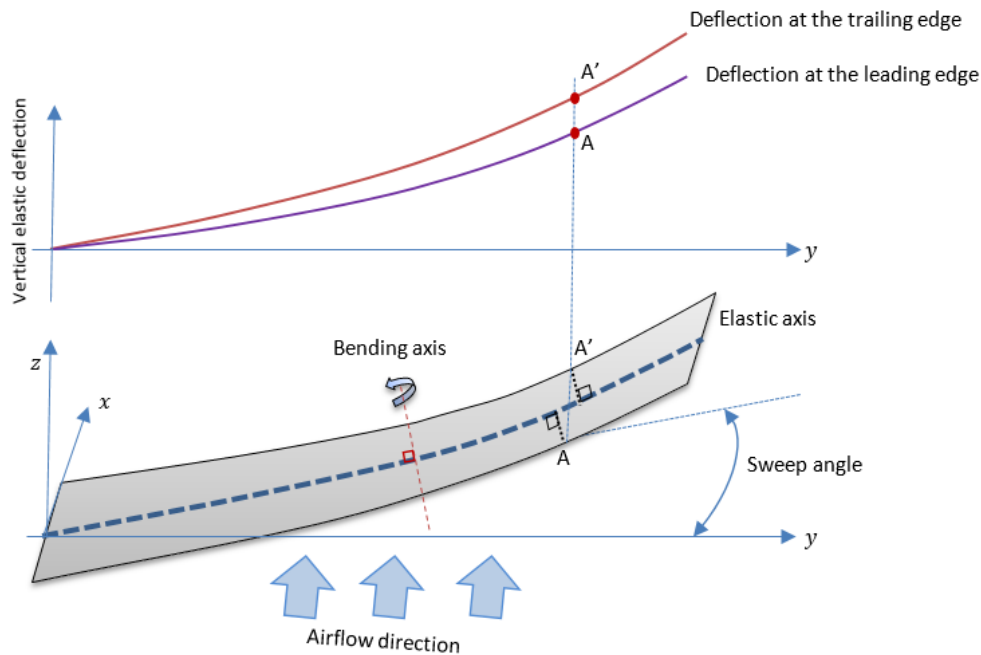


Figure 1: The elastic twist due to pure up-bending load of the swept flying wing

## 2. Methodology

The main target of this paper is to study how the spar location can influence the optimisation results of a solar powered high altitude aft-swept flying wing. The following steps were followed to conduct this research:

- 1- Define design cases with different spar locations.
- 2- Conduct the optimisation process for each design case to find the optimal manufactured twist required to obtain minimum drag coefficient at the trim condition with a reference lift coefficient of about 0.8.
- 3- Compare the aerodynamic and the structural performance characteristics.

## 3. Aircraft layout and its Components

An aft-swept, nontapered flying wing is adopted here such as that sketched in Figure 2. The main characteristics of the aircraft were designed using a conceptual design tool that was developed by the authors in previous studies. Mission requirements were adopted to design a solar power high altitude long endurance UAV operating over southern Iraq for a civil mission. More details can be found in references [9, 10, 12, 13]. The main characteristics of the aircraft are tabulated in Table 1. A portion of the wing has a 10-degree dihedral to achieve an initial static stability in the directional and the lateral modes. The weight of the wing itself including the weight of the aircraft system can modify the load distribution across the wing leading to a significant influence on the sizing process and the elastic behaviour of the wing [14]. The structural weight was estimated using empirical equations employed in the previous design stage as functions of the planform geometry of the wing. However, during the process conducted in this research, only the spar needs to be sized regarding the ultimate loads which are represented as a load factor of 3. Therefore, the location of the aircraft elements must be defined prior the spar sizing process. Moreover, the number of the spar segments along the spanwise direction and the location of the spar along the chordwise direction

must be known. Here, the spar location is defined as a ratio of the chord length ( $X_{spar}$ ). The aircraft elements and their locations are assumed as follows:

1. The span (wingtip to wingtip) is discretised into 28 segments. The length of each segment is 2.1 m except the four segments at each end of the wing which are 2.03 m long as shown in Figure 3. A square cross-section shape is adopted for the spar and hence its height and width are made equal to 0.8 of the maximum thickness of the wing section. Each span segment will be sized according to the maximum bending moment, shear force and torsional moment exerted on the spar segment.
2. Six electric motors are adopted for the propulsion system. Each motor has the same characteristic of that used in the Helios aircraft [15]. Each motor weighs about 6.7 kg including the gear box and propeller. The motors are distributed along the spanwise direction, three in each semi-span as shown in Figure 3. The mass centre of each unit is assumed to be at  $0.1x/c$  of the local chord in front of the leading edge as shown in Figure 4.
3. Four fuel cells are adopted, each one weighing about 100 kg including the maximum power point tracker MPPT. They are distributed spanwise to reduce the bending moment at the root section. The mass centre of each fuel cell is assumed to be coincident with the elastic axis of the spar to reduce local twisting.
4. The weight of the landing gears is discretised into five units of equal weight located under the excessively loaded points which are directly below the fuel cells and the payload as shown in Figure 3.
5. The non-spar elements are discretised into segments as well. The mass centre of each segment is assumed to coincide with the centroid of the shaded area of the wing section which is located at about  $0.4x/c$  as computed by AutoCAD.
6. Finally, the solar cells are discretised into strips along the spanwise direction and their mass centre coincides with the  $0.45x/c$  axis.

Table 1: The main characteristics of aircraft

Parameter	Value	Unit	Description
$AR$	19	-	Aspect ratio
$b$	58	m	Wingspan
TR	1	-	Taper ratio
$S$	177.053	m <sup>2</sup>	Planform area
$C_{av}$	3.052	m	Mean geometric chord
$A_{sc}$	142.527	m <sup>2</sup>	Total area of solar cells
$\Lambda$	9	degree	Quarter chord sweep angle
$\rho$	0.1382	kg/m <sup>3</sup>	ISA air density at an altitude of 17 km
$V_{\infty}$	30.538	m/s	True air speed at level flight
Re	$0.907 \times 10^6$	-	$C_{av}$ referenced Reynolds number at level flight
$C_{Lref}$	0.80	-	Aeroplane lift coefficient at cruise
$m$	931.27	kg	Total mass
$m_{af}$	314.41	kg	Airframe mass
$m_{fc}$	375.01	kg	Mass of all fuel cells
$m_{sc}$	35.63	kg	Mass of all solar panels
$m_{mppt}$	20.307	kg	Mass of all maximum power point trackers
$m_{prop}$	41.203	kg	Mass of propulsion system
$m_{av}$	27.94	kg	Mass of Avionics
$m_{lg}$	16.763	kg	Landing gear mass
$m_{payload}$	100	kg	Payload
$P_{pld}$	1250	W	Payload power consumption
$P_{elec\ tot}$	10.595	kW	Total electric power consumption in level flight
$E_{day\ density}$	33.37	MJ/m <sup>2</sup> /day	Solar radiation between 1 <sup>st</sup> April and 10 <sup>th</sup> September at a latitude of $31.01^{\circ}$ (Southern Iraq) at 17km altitude
$T_{day}$	12.32	hr	Reference daytime duration
ZMR-17	-	-	Aerofoil used in the entire wing, maximum thickness to chord ratio of 12.57% at 32% chord [16]

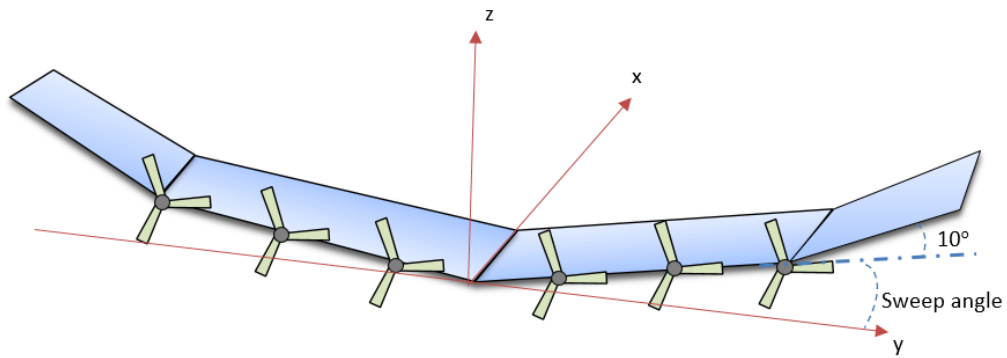


Figure 2: Initial layout of the aircraft

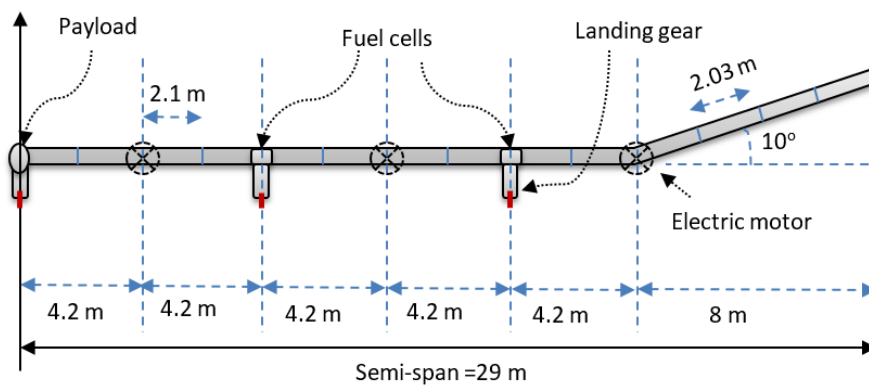


Figure 3: The front-side view of half wing of the aircraft and its weight distribution along the semi-spanwise direction

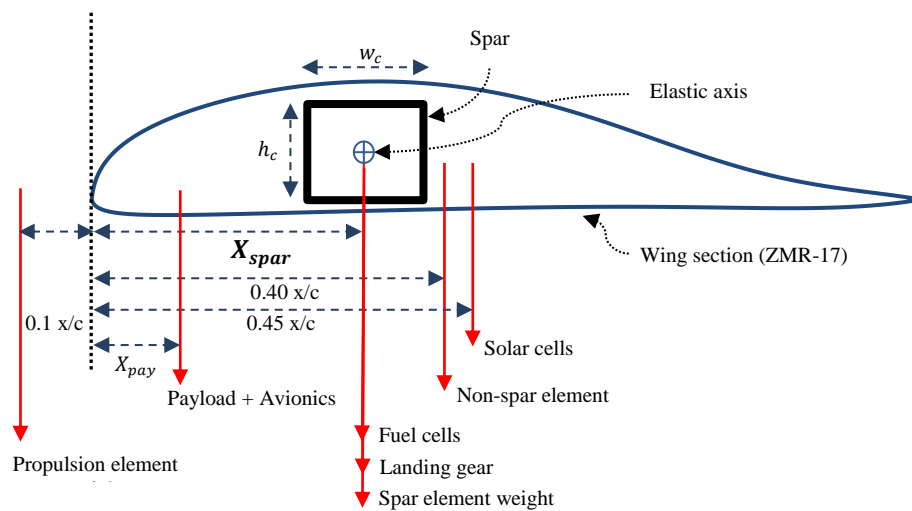


Figure 4: The weight distribution along the chordwise direction of the aircraft

## 4. Optimisation Tool

A design optimisation framework was developed within a MATLAB environment combining a quasi-3D aerodynamic model and a composite structure model.

The quasi-three-dimensional aerodynamic solver (Quasi-3DM) was built using the vortex lattice method coupled with a two-dimensional inviscid-viscous aerodynamic solver (2D IVM). The coefficients of the induced drag ( $C_{D_{in}}$ ), lift ( $C_L$ ) and pitching moment ( $C_M$ ) were calculated using the vortex lattice method whilst the profile drag coefficient ( $C_{D_{prof}}$ ) of the wing was calculated using that of the two-dimensional wing sections obtained by the 2D aerodynamic solver (2D IVM) using the Strip Method as detailed in [17]. The composite structure model (CSM) was developed to size the wing structure and evaluate the elastic deflection using linear finite beam element method. Empirical equations were used to evaluate the weight of the non-spar elements. A design tool was then developed within this composite structure model to size the spar section according to the critical loads as detailed in [12].

The built-in Interior Point Algorithm (IPA) in the MATLAB environment was used in the optimiser code. The IPA is a derivative-based algorithm which uses a polynomial time linear programming procedure and an interior point method. In this method, the values of the upper and lower bounds of the design variables can be defined whilst the stopping criterion can be set to either reach a maximum number of iterations or achieve a minimum tolerance of the objective function or the value of the variable.

Figure 5 shows an overview of the communication shape among the disciplinary models of the optimisation tool in which, for each iteration, three main steps are conducted:

### 1. Evaluate the critical aerodynamic loads and size the spar.

An angle of attack was chosen to evaluate the aerodynamic loads at the cruise condition for sizing purposes. The design cases performed prior this study indicated that the trim condition will occur at an angle of attack of around 7 or 8 degrees. If the total lift was not equal to the calculated weight, the aerodynamic loads will be multiplied by a factor to equalise the two forces. Then, the aerodynamic load will be multiplied by the load factor to evaluate the critical aerodynamic load. Subsequently, using the composite structure model, the spar will be sized. In this step, only one flow solution is needed while the sizing process will be repeated to employ the inertial relief of the spar weight until a solution that converges is achieved. The effects of static aeroelasticity are ignored at this stage.

### 2. Find the trim condition and its corresponding angle of attack

The aerodynamic performance parameters will be calculated at three angles of attack (AoAs): 1, 6 and 9 degrees. At each angle of attack, the coupling of the aerodynamic and the structural influences will be considered until achieving a solution which converges for elastic deformations. Then, the aerodynamic parameters at the three angles of attack will be used to calculate the angle of attack corresponding to the trim condition assuming that the curves [ $C_L$  versus  $\alpha$ ] and [ $C_M$  versus  $C_L$ ] are represented as polynomial equations. Moreover, the static longitudinal stability parameters  $\frac{\partial C_M}{\partial C_L}$  and  $C_{M_0}$  are then found.

### 3. Evaluate the aerodynamic performance parameters at the trim condition

The aerodynamic performance parameters of the flight shape at the trim condition are then calculated using the trimmed angle of attack ( $\alpha_{trim}$ ) obtained from the previous procedure.

The concept of the optimisation problem is to achieve the best possible result within the design space variables. Here, the design variables are the manufactured twist distribution which was represented by 14 twist angles for the inboard and outboard sections of the given wing partitions. The twist of the panels within each partition will be linear as shown in Figure 6.

The object of the optimisation is to achieve the minimum drag coefficient of the aircraft at the flight condition. It is necessary to enable the objective function to drive the optimisation process to achieve trim condition at the reference lift coefficient of 0.8 whilst maintaining the drag coefficient at the minimum value. Therefore, the objective function was modified to minimise the trimmed drag coefficient ( $C_{D_{trim}}$ ) in addition to reducing the difference between the achieved trimmed lift coefficient ( $C_{L_{trim}}$ ) and the reference lift coefficient ( $C_{L_{ref}}$ ). The optimisation problem can be formulated as:

*Objective:*

$$\text{minimise } (|C_{L_{ref}} - C_{L_{trim}}| + C_{D_{trim}})$$

*subject to:*

$$C_{M_{trim}} = 0, \quad \frac{\partial C_M}{\partial C_L} < 0, \quad C_{M_0} > 0$$

*Design variables:*

$$TW_1, TW_2, TW_3 \dots \dots \dots TW_{14}$$

where  $Tw_i$  are the manufactured twist distribution (as shown in Figure 6)

$$1^\circ > Tw_i > -5^\circ$$

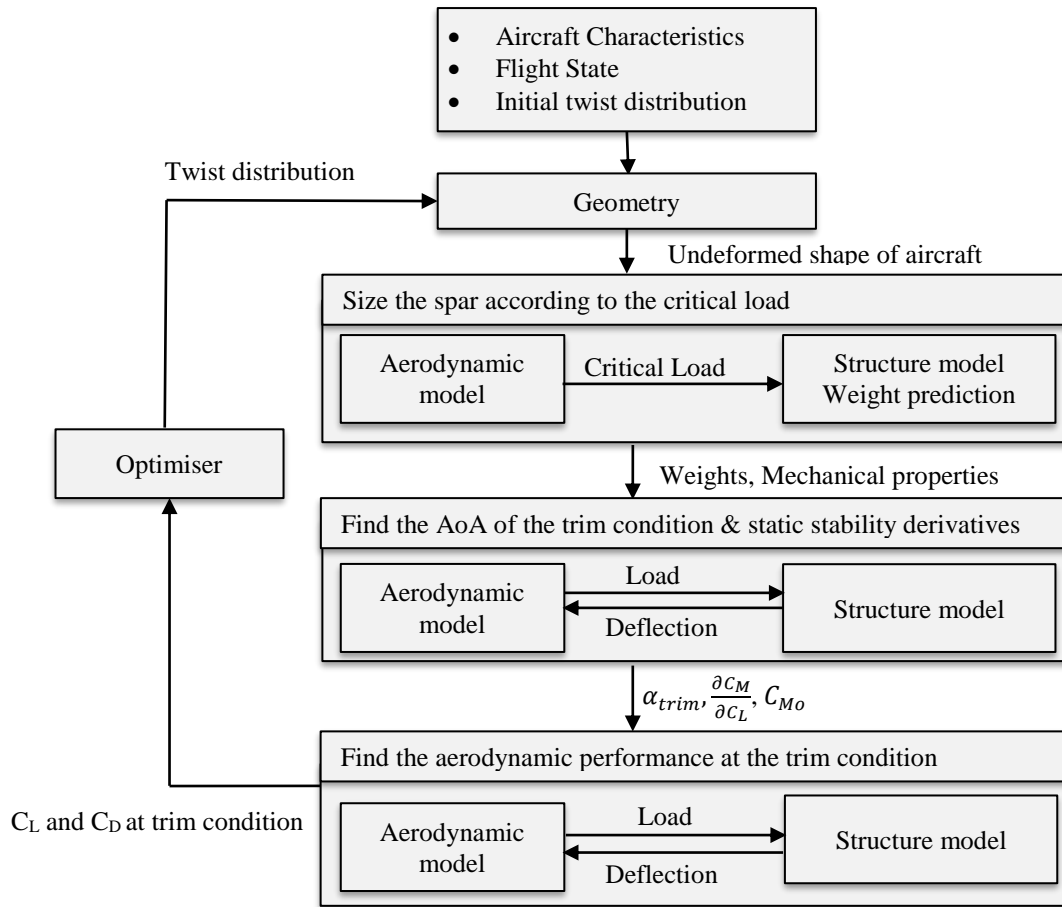


Figure 5: Framework of the optimisation tool

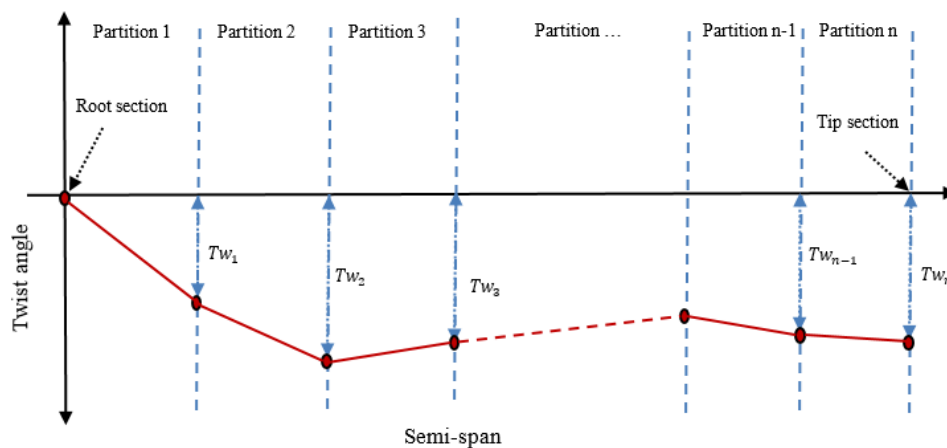


Figure 6: Manufactured twist distribution pattern

## 5. Spar Location Study

Four design cases have been introduced with the spar located at  $0.25x/c$ ,  $0.30x/c$ ,  $0.35x/c$  and  $0.4x/c$ . In each case, the optimisation tool was used to select the manufactured twist distribution for achieving minimum drag coefficient at a trimmed lift coefficient of 0.8. Care was taken to ensure that the fuel cells were always placed on the elastic axis of the spar to prevent local twist deformations. Moreover, the payload location was adjusted in every design case to achieve a specific static margin of about -0.05.

The optimisation process was conducted at each design case. The optimal manufactured twist distribution and the aerodynamic performance of the resulting cases are presented in Figure 7. The results indicate that the spar location has an enormous impact on the structural behaviour and hence the aerodynamic performance and stability. A significant influence can be seen in the lift slopes and the trimmed angle of attack. All the resulting cases were statically stable at the trim condition at the lift coefficient of 0.8. However, for cases where the spar was located at  $0.25x/c$  and  $0.3x/c$ , the system became unstable at lower angles of attack due to elastic deformations encountered as presented in Figure 8 and Figure 9.

The elastic twist distribution shown in Figure 8 was with respect to the flow direction indicating that this elastic twist was part of the total incidence change due to the local torque, and a part of the bending deflection due to the wing sweep. In order to better understand how the spar location can influence the wing, the essentials of the swept wing theory need to be invoked. For an aft-swept wing, in the case of up-bending load, the incidence angles will be reduced due to the bending of the spar. At the down-bending load, this behaviour will be reversed leading to an increase in the incidence angles. The aerodynamic torques (local pitching moments) about the elastic axis can worsen or reduce the change in the incidence.

For the Case1 with  $0.25x/c$  spar location, the elastic axis was located in front of the local aerodynamic centre which resulted in negative pitching moments about the elastic axis which tends to reduce the incidence at higher wing loading (higher angle of attack). At lower angles of attack, the negative lift will result in positive pitching moments which tend to increase the incidence angle. This will be more pronounced at the wing tips where the wash-out in the manufactured twist is exploited. It can be concluded that the vertical deflections will work in cooperation with the aerodynamic torque to worsen the elastic behaviour when the spar was located in front of the local aerodynamic centre. In the second case in which the spar was located at  $0.3x/c$ , the elastic twist is reduced due to reducing the aerodynamic torsions (pitching moments) about the elastic axis.

In Case4 with the spar located at  $0.4x/c$ , the behaviour of the elastic twist is reversed due to the elastic axis situated behind the local aerodynamic centre. At higher angles of attack, the aerodynamic torques tend to increase the incidence angles while the bending up of the wing tends to reduce it. The behaviour is reversed at the lower angles of attack. However, the local aerodynamic torques are increased which in turn necessitates a stiffer structure leading to increasing structural weight as indicated in Table 2. Accordingly, the stiffer structure led to reduced vertical deflection. This case produced the best aerodynamic performance and static stability compared with the other cases but at a heavier structural weight.

In Case3, with the spar located at  $0.35x/c$ , a compromise solution was reached at which the aerodynamic loads could mitigate the twist due to the bending deformation. This choice led to a reduction in the change of the elastic twist with increasing wing loading. Also, the location of the spar was adjacent to the maximum thickness of the wing sections.

Table 2: The aerodynamic performance at the trim condition of the spar locations study

Cases	Spar locus $x/c$	Aerodynamic performance at trim condition ( $C_L = 0.8$ )					$\alpha_{trim}$ [deg.]	$C_{M0}$	Gross Weight [kg]
		$C_{D_{prof}}$	$C_{D_{in}}$	$C_D$	$\frac{C_L}{C_D}$	$\frac{\partial C_M}{\partial C_L}$			
Case 1	0.25	0.008140	0.010757	0.01889	42.33	-0.0522	7.2626	-0.0001	874.23
Case 2	0.30	0.008132	0.010657	0.01879	42.58	-0.0558	7.1478	0.0076	872.28
Case 3	0.35	0.008115	0.01058	0.01870	42.77	-0.0524	8.1376	0.0158	900.04
Case 4	0.40	0.007816	0.010704	0.01852	43.19	-0.0479	6.4874	0.0204	977.42

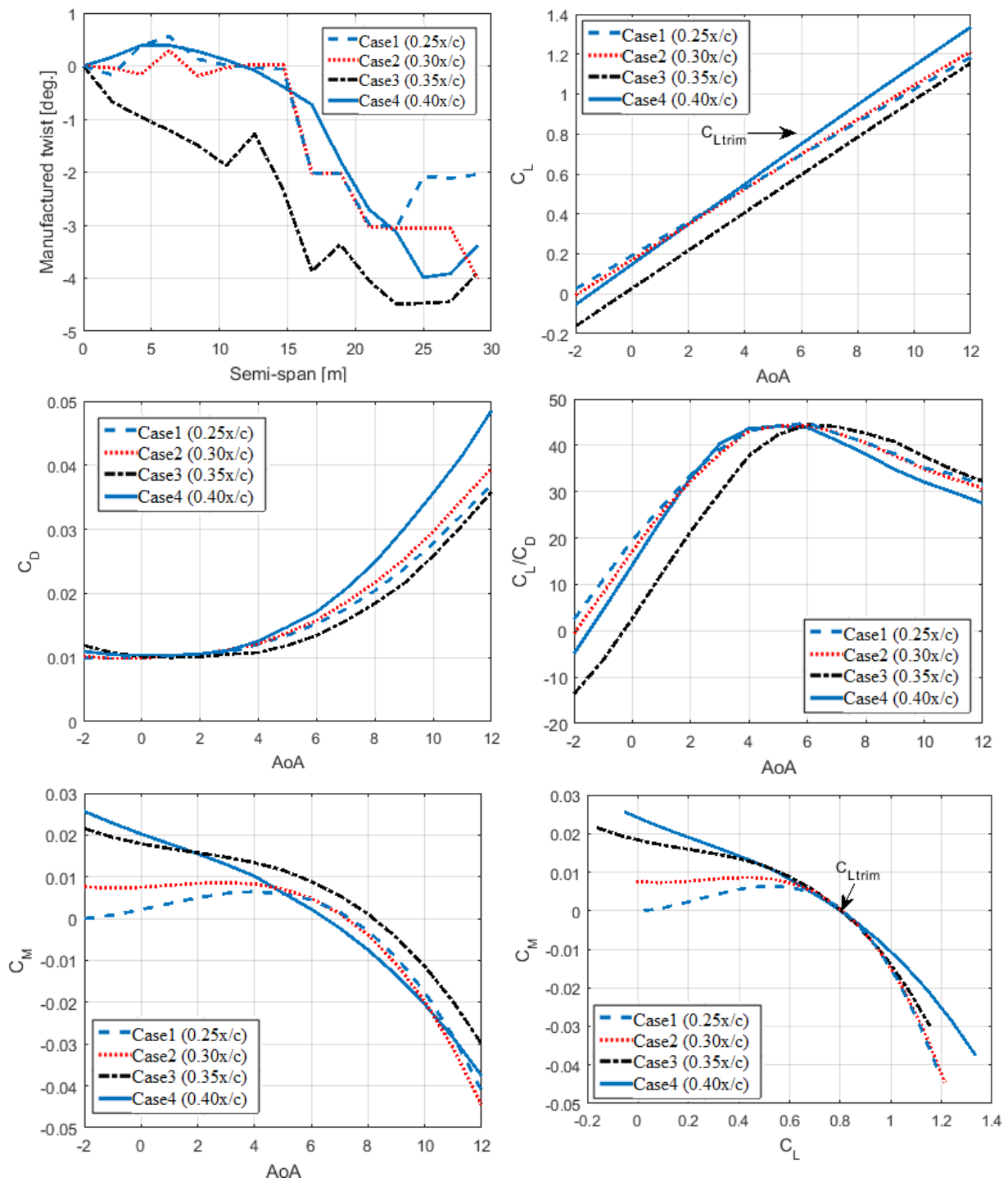


Figure 7: The influence of the spar location on the aerodynamic performance of the resulted cases.

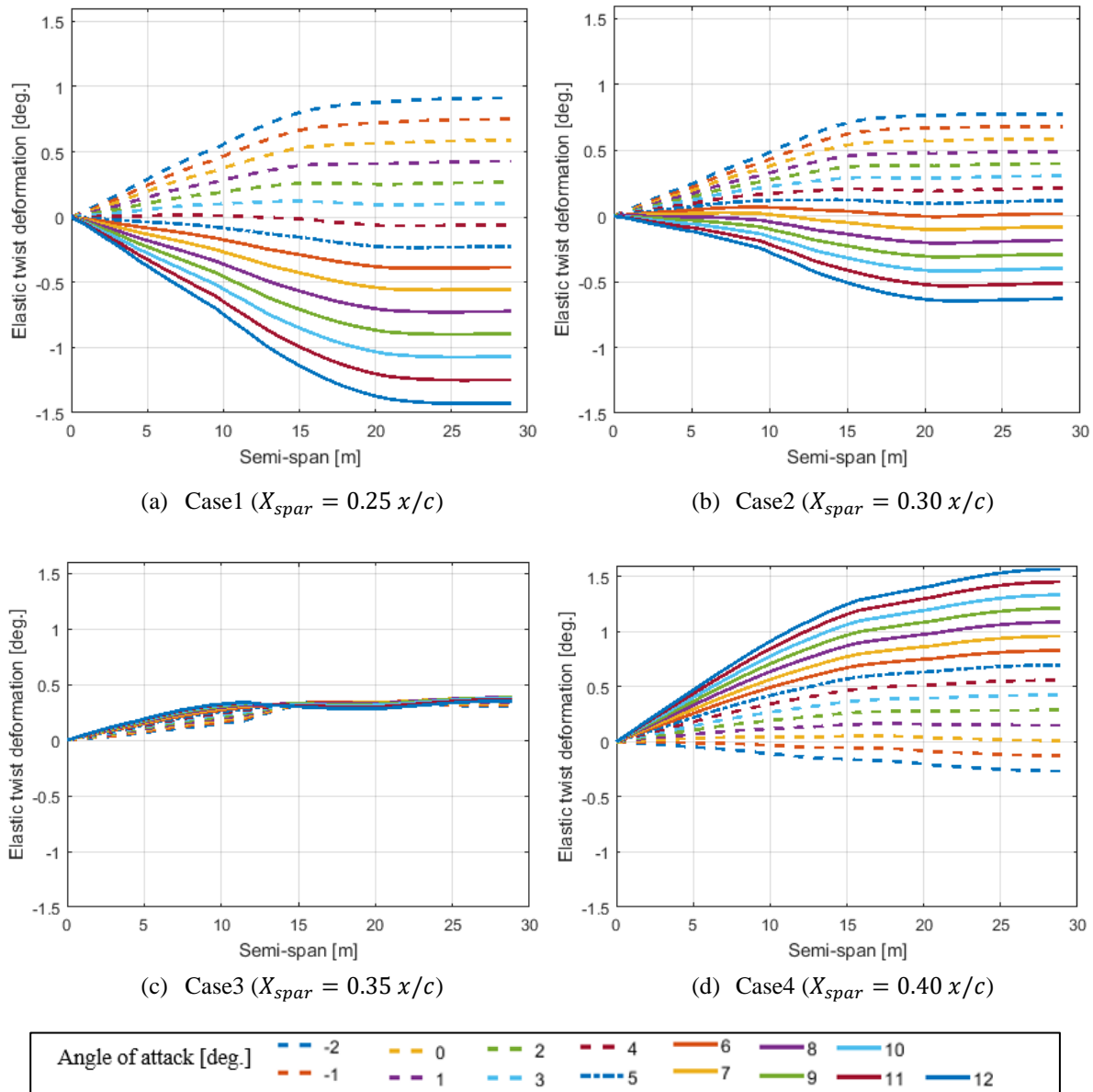


Figure 8: The effect of the spar location on the elastic twist (respect to the flow direction) of the resulted cases.

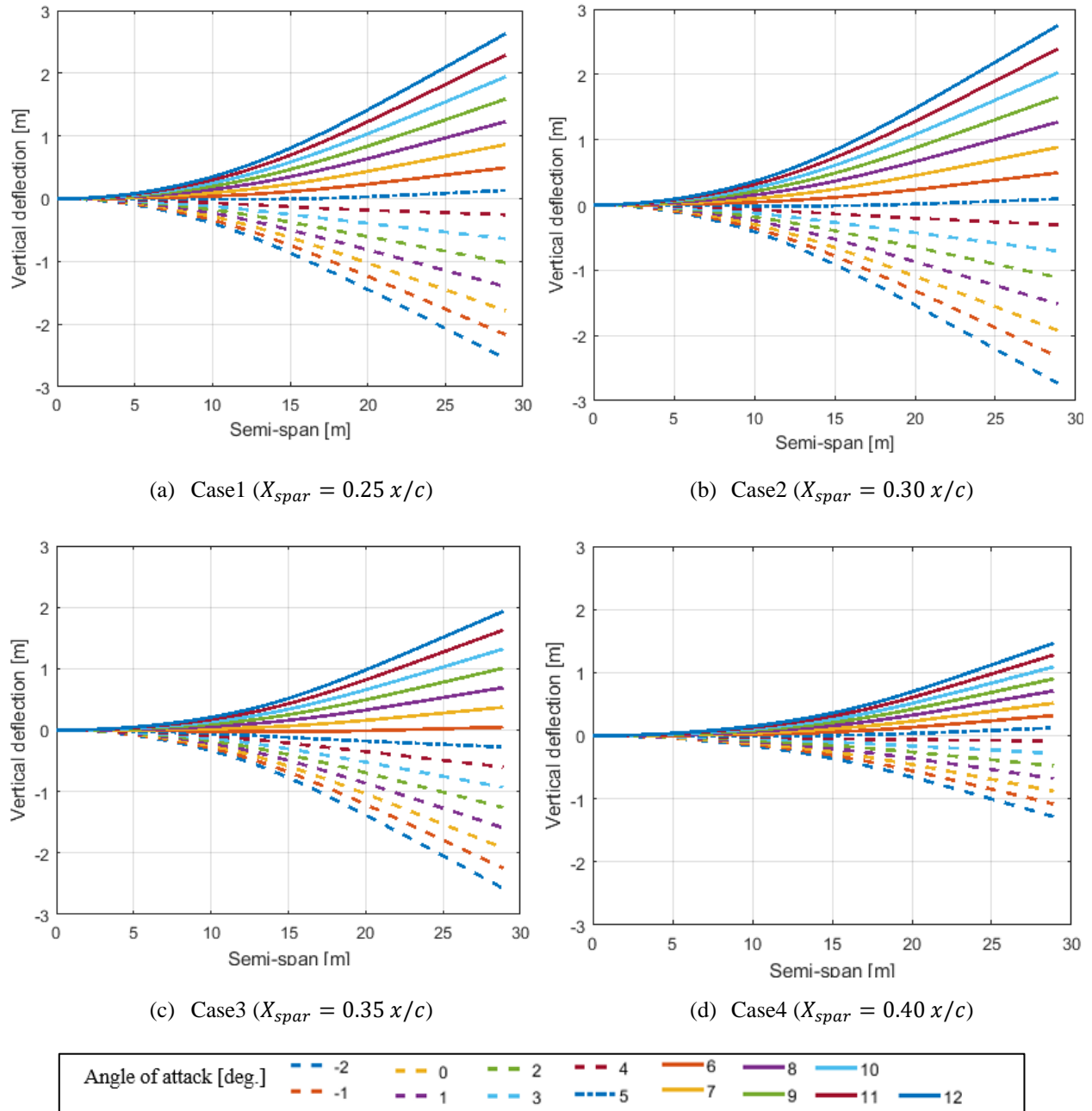


Figure 9: The effect of the spar location on the elastic vertical deflection of the resulted cases

## 6. Conclusion

Four different cases with different spar locations were designed using a multidisciplinary design tool. The optimal manufacturing twist distribution for each design case was found for minimum drag coefficient at the trim condition. The aerodynamic and the structural performance figures for the resulting solution were evaluated and compared at different angles of attack. The results indicate that, if the spar location was behind the aerodynamic centre, it can reduce the deformation in the twist during cruise. In other words, the aerodynamic loads, particularly the pitching moment, can twist the wing in either a beneficial or a detrimental manner when the wing bends. This needs to be borne in mind before the optimisation process in which the required manufactural twist distribution would result in a trimmed flight condition at a specific lift coefficient. The optimal location of the spar can be varied depending on several limitations such as the weight distribution in multiple directions, the aerofoil shape and the location of the maximum wing thickness along with the sweep angles and the required static margin. Employing the spar location as

a variable in the optimisation process would be useful for further work but additional constraints such as the limit of the structural weight and the static stability at lower angles of attack will need to be considered.

## 7. Acknowledgment

The authors would like to thank the Higher Committee for Education Development in Iraq (HCED-Iraq) for supporting this research at University of Salford.

## References

1. Houghton, E.L. and P.W. Carpenter, *Aerodynamics for Engineering Students*, 5Ed. ISBN 0 7506 5111 3, 2003.
2. Wang, Z., et al., Nonlinear-Aerodynamics/Nonlinear-Structure Interaction Methodology for a High-Altitude Long-Endurance Wing. *Journal of Aircraft*, 2010. 47(2): p. 556-566.
3. Cesnik, C.E. and W. Su. Nonlinear aeroelastic simulation of X-HALE: a very flexible UAV. in 49th AIAA Aerospace Sciences Meeting including the New Horizons Forum and Aerospace Exposition, Orlando, Florida. 2011.
4. Cesnik, C.E., et al., X-HALE: a very flexible UAV for nonlinear aeroelastic tests. Paper No. AIAA-2010-2715, *Proceedings of (2010)*, 2010.
5. Vasiliev, V.V. and E. Morozov, *Advanced mechanics of composite materials and structural elements*. 2013: Newnes.
6. Raghavan, B., *Flight dynamics and control of highly flexible flying-wings*. 2009.
7. Lee, G., Tailless aircraft design problems. *The Aeronautical Journal*, 1947. 51(434): p. 109-131.
8. Skoog, R.B., *An analysis of the effects of aeroelasticity on static longitudinal stability and control of a swept-wing airplane*. 1957.
9. Alsahlani, A. and T. Rahulan. Conceptual and Preliminary Design Approach of A High Altitude, Long Endurance Solar-Powered UAVs. in *CSE Annual PGR Symposium (CSE-PGSym 17)*. 2017. Salford, UK: University of Salford
10. Alsahlani, A. and T. Rahulan. The impact of altitude, latitude, and endurance duration on the Design of a High Altitude, Solar Powered Unmanned Aerial Vehicle. in *International Conference for Students on Applied Engineering (ISCAE), IEEE*. 2016. Newcastle / UK: IEEE.
11. Alsahlani, A., L.J. Johnston, and P.A. Atcliffe, Design of a High Altitude Long Endurance Flying-wing Solar-Powered Unmanned Air Vehicle. *Progress in Flight Physics*, 2015. 0: p. 0.
12. Alsahlani, A., T. Rahulan, and N. Abdulhassan, Composite Structural Analysis of a High Altitude, Solar Powered Unmanned Aerial Vehicle. *International Journal of Mechanical Engineering and Robotics Research, IJMERR*, 2017. 6(1): p. 71-76.
13. Alsahlani, A. and T. Rahulan, Weight Estimation of a Conceptual Wing for a High Altitude, Solar Powered Unmanned Aerial Vehicle, in *5th Aircraft Structural Design Conference 2016*, The Royal Aeronautical Society: Manchester / UK.
14. Torenbeek, E., *Advanced Aircraft Design: Conceptual Design, Technology and Optimization of Subsonic Civil Airplanes*. 2013: John Wiley & Sons.
15. Noll, T.E., et al., *Investigation of the Helios Prototype Aircraft*, T.H.M.I. Board, Editor. 2004.
16. Alsahlani, A. and T. Rahulan, Aerofoil Design for Unmanned High-Altitude Aft-swept Flying-Wings. *Journal of Aerospace Technology and Management*, 2017.
17. Alsahlani, A., L.J. Johnston, and P.A. Atcliffe, Design of a High Altitude Long Endurance Flying-wing Solar-Powered Unmanned Air Vehicle, in *6TH European Conference for Aeronautics and Space Sciences (EUCASS2015)*. 2015, EUCASS: Krakow, Poland.